FARADAY

Mechanism of the electrochemical reduction of carbon dioxide at inert electrodes in media of low proton availability

Armando Gennaro,[a] Abdirisak A. Isse,[a] Maria-Gabriella Severin,[a] Elio Vianello,[a]* Iqbal Bhugun[b] and Jean-Michel Savéant[b]*

[a] *Istituto di Chimica Fisica, Università di Padova, Via Loredan 2, 35131 Padova, Italy*
[b] *Laboratoire d'Electrochimie Moléculaire de l'Université Denis Diderot (Paris 7), 2 place Jussieu, 75251 Paris Cedex 05, France*

Direct electrolysis of CO_2 in DMF at an inert electrode, such as mercury, produces mixtures of CO and oxalate, whereas electrolysis catalysed by radical anions of aromatic esters and nitriles produces exclusively oxalate in the same medium. Examination of previous results concerning the direct electrochemical reduction and the reduction by photoinjected electrons reveals that there are no significant specific interactions between reactant, intermediates and products on the one hand, and the electrode material on the other, when this is Hg or Pb. These observations and a systematic study of the variations of the oxalate and CO yields with temperature and CO_2 concentration, allow the derivation of a consistent mechanistic model of the direct electrochemical reduction. It involves the formation of oxalate from the coupling of two CO_2 radical anions in solution. CO (and an equimolar amount of carbonate) is produced by reduction at the electrode of a CO_2–$CO_2^{\bullet -}$ adduct, the formation of which, at the electrode surface, is rendered exothermic by non-specific electrostatic interactions.

Albeit a very stable molecule, carbon dioxide plays the role of a carbon source in essential natural processes. Among the artificial modes of activating this molecule, much attention has been devoted to electrochemical activation. The electrochemical generation of the CO_2 radical anion requires a fairly negative potential (the standard potential of the $CO_2/CO_2^{\bullet -}$ couple in *N*,*N*'-dimethylformamide (DMF) with 0.1 mol dm^{-3} NEt_4ClO_4 as supporting electrolyte has been estimated to be −2.21 V *vs.* SCE by cyclic voltammetry on a mercury electrode.[1] The products of the direct electrochemical reduction depend on both the chemical nature of the electrode and the reaction medium. In low acidity solvents, such as DMF, and with a mercury or lead electrode, the reduction takes place at potentials around the standard potential of the $CO_2/CO_2^{\bullet -}$ couple indicating that the interactions between the electrode and the reactant, intermediates and products are weak. At such inert (or outersphere) electrodes, the reduction products are oxalate and carbon monoxide when the solvent is dry.[2,3] Similar results were found in other aprotic solvents at Hg, Pb and Tl electrodes.[3,4] The relative amounts of oxalate and carbon monoxide depend upon current density and CO_2 concentration, and the presence of water promotes the formation of formate.[2] Other metals presumably play a catalytic role through chemisorption of CO_2, intermediates or products. CO is then the main product as with Au, Pt, Ag and Cu in propylene carbonate.[4] This is also the case with Au, Sn, Cd and Zn layers freshly deposited on the electrode surface in DMF or *N*-methylpyrrolidone.[5]

In water, high yields of formic acid may be obtained as discovered many years ago[6–8] and confirmed by more recent studies.[9] However, the product distribution depends considerably upon the nature of the electrode material and the reaction medium, and chemisorption of intermediates and/or products also probably plays a crucial role. Besides formate and CO.[10,11] other products such as formaldehyde,[12] methanol[13,14] and methane[10,14–18] can be formed. It is however, interesting to note that on an inert electrode such as lead, one obtains, with a large overpotential, solely formate,[19] as expected from the results obtained in DMF. On the other hand, oxalate, partially reduced to glyoxalate, is formed, together with formate, on mercury in the presence of quaternary ammonium salts, again with a large overpotential.[20,21]

The product distribution found in DMF at inert electrodes such as Hg and Pb, and its variations with current density and CO_2 concentration suggested the mechanism depicted in Scheme 1.[2,22–24] Oxalate is considered to be formed from the coupling of two radial anions [reacton (1)] while the production of CO, and of an equimolar amount of carbonate, involves, as intermediate, an adduct between CO_2 and its radical anion where the C—O bond formed results from the donation of an electron pair from the latter to the former [reaction (2)]. The secondary radical anion thus produced may successively undergo electron transfer from the electrode or from the primary radical anion accompanied by the breaking of one of the C— bonds of the primary radical anion to yield CO and carbonate [reactions (3) and (3')]. The formation of formate involves the water that is present which may protonate $CO_2^{\bullet -}$ leading to a neutral radical [reaction (4)]

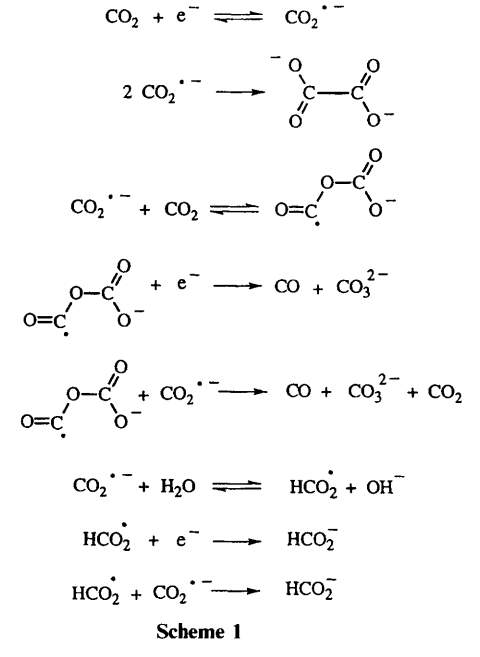

Scheme 1

from which formate is derived after an additional electron transfer step [reactions (5) and (5')].

It has been found recently that radical anions of aromatic esters and nitriles may be used to catalyse homogeneously the electrochemical reduction of CO_2.[25] Over an extended range of concentration and temperature, the only reduction product is oxalate while no detectable amounts of CO are formed. This striking difference in product distribution between the direct and homogeneously catalysed reactions prompted us to re-examine the mechanism of the direct electrochemical reduction of CO_2 at inert electrodes. For this reason we analysed in a more systematic manner the effect of CO_2 concentration on product distribution. We also investigated the effect of temperature. The discussion will take into account the contention, based on Tafel plots and photoemission experiments, that specific adsorption is an essential factor of the reduction mechanism, even for electrodes previously presumed inert such as mercury and lead, in water[26] as well as in aprotic solvents.[27] The main questions to be addressed are: is the product distribution entirely controlled by homogeneous follow-up reactions; is the electrode surface playing a specific (chemical) role?

Experimental

Chemicals

DMF (Carlo Erba, RPE) was kept over anhydrous Na_2CO_3 for several days and stirred occasionally. It was then fractionally distilled under reduced pressure under N_2 twice and stored in a dark bottle under N_2. In order to remove as much residual water as possible the solvent was repeatedly percolated before use through a column of neutral alumina (Merck, activity grade 1) previously activated overnight at 360 °C under vacuum. Tetrabutylammonium perchlorate (Fluka purum) was recrystallized twice from a 2 : 1 water–ethanol mixture and then dried in a vacuum oven at 60 °C. CO_2 (99.998%) was supplied by SIAD (Italy). The solubility of the gas in DMF (0.199 mol dm^{-3} at 25 °C and 1 atm pressure) at various temperatures and various partial pressures has been reported previously.[28] DMF solutions containing various concentrations of CO_2 were prepared by saturating the solvent with appropriate mixtures of CO_2 and argon. The apparatus used for the preparation of the gas mixtures and the method of calculating CO_2 concentrations in the solution from its partial pressure in the gas phase have been described previously.[28]

Electrochemical instrumentation and procedures

Cyclic voltammetric measurements were made with a PAR Model 173 potentiostat or with a home-built potentiostat equipped with positive feedback compensation,[29] a programmable function generator Amel or a Model 568 EGG PAR 175 signal generator and a 2090 Nicolet oscilloscope. An Amel Model 863 *X–Y* recorder or an IFELEC 2502 chart recorder were used for recording the cyclic voltammograms. A mercury micro-electrode was used as working electrode and a platinum wire as counter-electrode. The working electrode was made from a 2 mm diameter platinum sphere coated with mercury after electrolytic deposition of silver or a 1 mm diameter gold disk coated with mercury. The reference electrode was Ag/AgI/Bu_4NI (0.1 mol dm^{-3} in DMF) whose potential was always compared with that of the SCE to which all potentials are finally referred. Both the reference and the counter-electrodes were separated from the working-electrode compartment by glass frits and salt bridges.

The diffusion coefficient of CO_2 in DMF has been found previously to be 2.7×10^{-5} cm^2 s^{-1}.[30] For the catalyst we have found an average value of 0.8×10^{-5} cm^2 s^{-1}. These values were used in the construction of the working curves for extracting the rate constants from the cyclic voltammetric data.

Preparative scale experiments were performed in a gas-tight electrolysis cell under galvanostatic conditions with a current density of 1.6 mA cm^{-2}. Before starting the electrolysis, a solution saturated either with CO_2 alone or with a mixture of CO_2 and argon was prepared by bubbling the gas into the catholyte for *ca.* 30 min. During electrolysis, the cell was maintained in contact with a gas reservoir containing CO_2 at the appropriate partial pressure. A mercury pool of 12.4 cm^{-2} was used as cathode. The same stirring rate was used in all the experiments in order to achieve reproducible hydrodynamic conditions.

Electrolysis products present both in the gas and liquid phases were analysed by chromatographic techniques. Carbon monoxide and formic acid were analysed on a Varian 3700 gas chromatograph equipped with a thermal conductivity detector, using helium as the carrier gas. CO was analysed only in the gas phase using a molecular sieve column. Since the solubility of CO in dipolar aprotic solvents is very low,[31,32] the quantity of CO present in solution was considered to be negligible. Samples were extracted from the gas phase of the working electrode compartment with a gas syringe through a septum cap. To detect formate, the solution was first esterified by addition of methyl iodide to a portion of the electrolysed solution.[33] The resulting solution in DMF was then analysed by GC using a G 10% SP-1200, 1% H_3PO_4 Supelco column. Oxalate was directly analysed in HPLC with a Perkin Elmer Series 4 liquid chromatograph equipped with a UV detector operating at 210 nm, using an Aminex HPX-87H ion-exchange column eluted with 0.005 mol dm^{-3} H_2SO_4 on which conversion of oxalate to oxalic acid takes place. The validity of this procedure was checked by comparison with the classical permanganate colorimetric method.[34]

Results

Fig. 1 shows a typical cyclic voltammogram of CO_2 in DMF. The cathodic peak remains irreversible up to 1000 V s^{-1}. The peak width indicates that electron transfer is rate-controlling with a transfer coefficient close to 0.5 (0.55). It has been reported that some reversibility appears at a high scan rate (4400 V s^{-1}) from which an approximate estimate of the standard potential of the $CO_2/CO_2^{\cdot -}$ couple (−2.21 V *vs.* SCE in DMF +0.1 mol dm^{-3} Bu_4NClO_4) was derived.[1] In the original publication, a rough estimate of 10^7 mol dm^3 s^{-1} was given for the dimerization rate constant [reaction (1)]. A more accurate simulation of the cyclic voltammogram, taking account of the large double layer charging current, and of the exact value of the potential where the scan is reverted not far

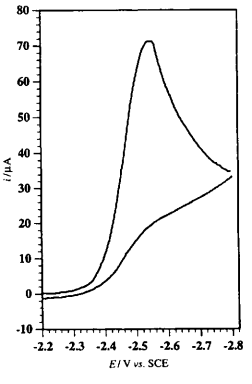

Fig. 1 Cyclic voltammetry of CO_2 (1.36 mmol dm^{-3}) in DMF (+0.1 mol dm^{-3} Bu_4NClO_4) at a mercury electrode. Scan rate: 0.1 V s^{-1} Temp.: 25 °C.

from the foot of the cathodic, gives a value of 5×10^8 mol^{-1} dm^3 s^{-1}. The number of electrons per molecule is close to 1 when $[CO_2] > 5$ mmol dm^{-3}, a stoichiometry that agrees with the formation of oxalate as well as the formation of CO (and carbonate). The number of electrons per molecule increases, 'plateauing' at a value of 2, upon decreasing the CO_2 concentration. The change in the electron stoichiometry is most likely related to the increasing interference of $CO_2^{\bullet -}$ protonation by residual water [reaction (4)] and of the ensuing electron transfer reactions (5) and/or (5').

Upon raising the concentration of CO_2 to the saturation value (0.231 mol dm^{-3}), the shape of the voltammogram remains unchanged and the peak current is proportional to concentration (Fig. 2) provided that the ohmic drop is carefully compensated for by means of a positive feedback device.[29] The shape of the voltammograms indicates that the current is jointly governed by diffusion and by the irreversible kinetics of the initial electron uptake.[35]

These conclusions are at variance with those of an earlier investigation of the reaction in acetonitrile at a low scan rate (20 mV).[27] log(current) *vs.* potential plots (Tafel plots) exhibit two successive straight lines of different slopes that were assigned to two successive electrode reactions. We suspect non-compensated ohmic drop to be responsible for this behaviour as illustrated in Fig. 3 where Tafel plots obtained in the same solvent, at the same scan rate, with and without compensation of the ohmic drop are shown. Because the scan rate is low, the diffusion of species to and from the electrode is not semi-infinite but takes place within a steady-state diffusion layer arising from natural convection (see ref. 36 and references therein). The consequence is that the voltammograms, unlike those obtained at higher scan rates (Fig. 1 and 2), are plateau-shaped (as rotating disk electrode voltammograms) rather than peak-shaped. When ohmic drop is correctly compensated for, the Tafel transformation of the voltammogram exhibits first a linear section with a 1/95 mV slope where the current is governed by the rate of electron transfer. Beyond the peak, the current plateaus at a value, i_l, representative of mass transport (diffusion + convection) of CO_2 toward the surface. In the absence of ohmic drop compensation, the increasing interference of ohmic drop delays the appearance of mass transport control. As the potential becomes more and more negative, the increase in the reduction current is increasingly compensated for by a parallel increase in the ohmic drop, thus decreasing the slope of the log i *vs.* E plot before the limiting current, i_l, is eventually reached. Under such conditions, the Tafel plot is well simulated by the equation, $-2.21 - Ri - 0.095 \log i + 0.095 \log(i_l - i)$ (E in V *vs.* SCE, I in A) where $R = 140\ \Omega$, and $\log i_l = -2.95$ as seen in Fig. 3, where we have also shown how such a Tafel plot can be con-

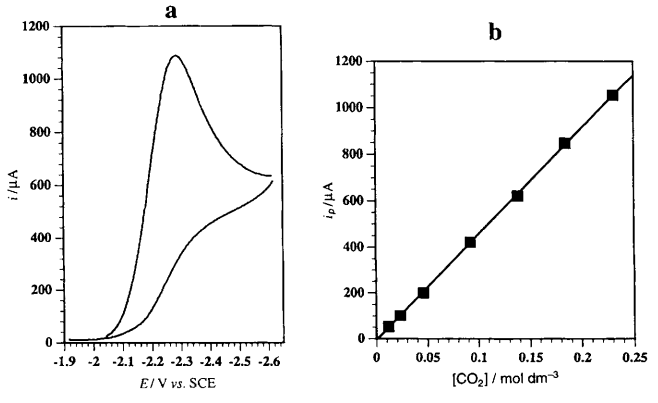

Fig. 2 Cyclic voltammetry of CO_2 in DMF (+0.1 mol dm^{-3} Et_4NClO_4) at a mercury electrode (1 mm diameter) as a function of concentration. a: voltammogram at the saturation concentration (0.231 mol dm^{-3}). b: variation of the peak current with CO_2 concentration. Scan rate: 0.1 V s^{-1}. Temp.: 20 °C.

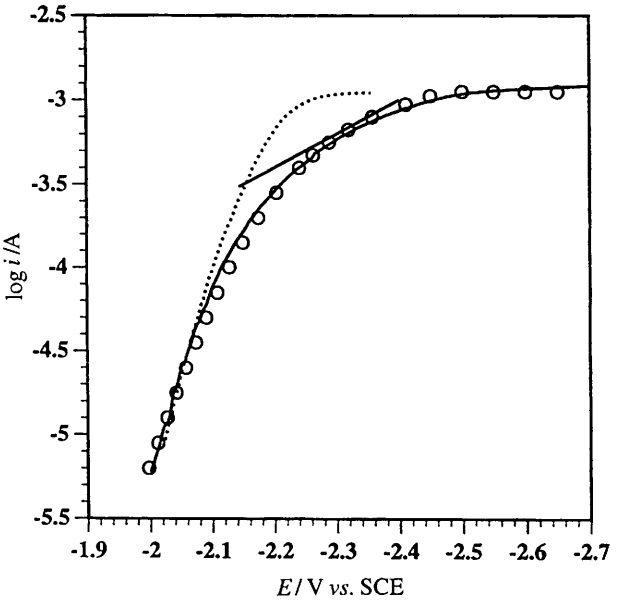

Fig. 3 Tafel plots for the reduction of CO_2 in CH_3CN (+0.1 mol dm^{-3} Et_4NClO_4) at a mercury electrode. Temp.: 25 °C. CO_2 conc. 0.2 mol dm^{-3}. Scan rate: 0.02 V s^{-1}. Dotted line: with positive feedback compensation of the ohmic drop; full line: without compensation. The open circles represent the fitting of the Tafel plot for the uncompensated current–potential curve with the equation $-2.21 - Ri - 0.095 \log i + 0.095 \log(i_l - i)$, $R = 140\ \Omega$, $\log i_l = -2.95$.

fused with two successive straight lines, giving the impression of two successive electrode reactions.

Since the current–potential responses are governed by diffusion and by the irreversible kinetics of the initial electron transfer, cyclic voltammetry, as with any other non-destructive interrogation of the reaction, provides scarce information on the follow-up steps, particularly on the competition between the pathways that lead from the initial radical anion to the final products (Scheme 1).

Analysis of the product distribution upon preparative-scale electrolysis was then necessary to get additional mechanistic information. In order to simplify the problem we have reduced the water content of the solvent down to levels (see Experimental section) where the production of formate is negligible. Most experiments were carried out at mercury, taken as a prototype of a presumably inert electrode at a low current density (1.6 mA cm^{-2}). The product distributions obtained at 25 °C and at lower temperatures are listed in Table 1. One

Table 1 Variation of product distribution with temperature in direct electrochemical constant current reduction of CO_2 in DMF (+0.2 mol dm^{-3} Bu_4NClO_4) at a mercury electrode[a]

temperature /°C	$[CO_2]$ /mmol dm^{-3}	$CO_2O_4^{2-}$ (%)[b]	CO (%)[b]	R_{CO}[c]	$R_{C_2O_4^{2-}}$[d]
25	152	67	25	0.27	0.73
	102	57	14	0.20	0.80
[e]	199	1.4	82	0.98	0.02
[f]	101	3.5	91	0.96	0.04
10	152	43	49	0.53	0.47
	102	56	33	0.37	0.63
0	152	33	64	0.66	0.34
	102	42	48	0.54	0.46
−10	152	22	75	0.77	0.23
	102	23	69	0.75	0.25
−20	152	11	89	0.89	0.11
	102	19	77	0.80	0.20

[a] Unless otherwise stated.[b] With respect to the total quantity of electricity consumed. [c] $R_{CO} = CO(\%)/[CO(\%) + C_2O_4^{2-}(\%)]$: CO yield with respect to the total quantity of CO and oxalate. [d] $R_{C_2O_4^{2-}} = C_2O_4^{2-}(\%)/[CO(\%) + C_2O_4^{2-}(\%)]$: oxalate yield with respect to the total quantity of CO and oxalate. [e] Gold. [f] Platinum.

Table 2 Variation of product distribution with concentration in direct electrochemical constant current reduction of CO_2 in DMF (+0.2 mol dm^{-3} Bu_4NClO_4) at a mercury electrode at 0 °C

$[CO_2]$ /mmol dm^{-3}	$C_2O_4^{2-}$ (%)[a]	CO (%)[a]	R_{CO}[b]	$R_{C_2O_4^{2-}}$[c]
20	89	10	0.10	0.90
30	80	12	0.13	0.87
42	74	26	0.26	0.74
55	66	34	0.34	0.66
75	49	46	0.48	0.52
102	42	48	0.54	0.46
152	33	64	0.66	0.44
217	23	76	0.77	0.23

[a] With respect to the total quantity of electricity consumed. [b] R_{CO} = CO(%)/[CO(%) + $C_2O_4^{2-}$(%)]: CO yield with respect to the total quantity of CO and oxylate. [c] $R_{C_2O_4^{2-}}$/[CO(%) + $C_2O_4^{2-}$(%)]: oxalate yield with respect to the total quantity of CO and oxalate.

notes a steady increase of the CO yield, and a converse decrease of the oxalate yield, upon decreasing temperature.

From the results in Table 1 where, at each temperature, the product distribution was determined for two concentrations, it is already apparent that the yield in CO decreases (and conversely, the oxalate yield increases) as the CO_2 concentration decreases. We have investigated this concentration dependence in more detail at 0 °C, as reported in Table 2, and observed steady increase in the CO yield with CO_2 concentration.

Discussion

One of the most striking features of the product distribution obtained from homogeneous catalysis by aromatic ester and nitrile radical anions is the almost total absence of CO formation[25] as opposed to direct electrolysis where CO and oxalate are formed in variable amounts according to the CO_2 concentration and the temperature. It is also worth noting that at platinum and gold electrodes (which are metals known to adsorb CO) CO is the only electrolysis product (Table 1). The mechanism of homogeneous catalysis by aromatic ester and nitrile radical anions is as depicted in Scheme 2, where P and Q represent the oxidized and reduced forms of the catalyst couple, respectively. The rate constants of reaction (0′) were determined in an extended series of aromatic ester and nitrile catalysts. The product distribution was rationalized by the fact that, in its competition with the dimerization step ($k_1 = 5 \times 10^8$ mol^{-1} dm^3 s^{-1}), the CO-forming path lacks efficiency both because the formation of $CO_2^{\bullet -}$–CO_2 [reaction (2)] is not thermodynamically very favourable ($K_2 \approx 0.07$ mol^{-1} dm^3) and its reduction by Q [reaction (3″)] is not very fast [only *ca.* 100 times faster than reaction (0)]. Under these conditions, the competition parameter, $\rho^{cat} = K_2 k_{3''} k_1^{-1/2} k_{0'}^{-3/4} [CO_2]^{1/4} (I/FD^{1/2})^{1/2}$ (I is the current density, D the diffusion coefficient of CO_2) is smaller than 10^{-2}, thus matching the observation that the faradaic yield of CO is less than 1%.

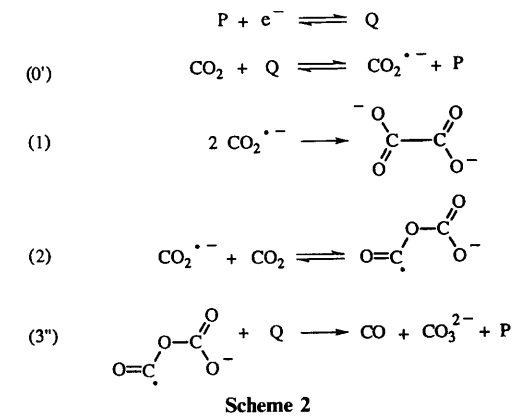

Scheme 2

Why is product distribution in direct electrolyses much more in favour of the formation of carbon monoxide than in homogeneous catalysis? What are the reasons for the observed variations of product distribution in direct electrolyses with CO_2 concentration and temperature (Tables 1 and 2)?

Previous preparative-scale studies in DMF at mercury and lead electrodes also revealed the formation of both oxalate and CO.[2,3] They have been rationalized in the framework of the mechanism depicted in Scheme 1 where the dimerization and adduct formation steps following first electron transfer were assumed to occur homogeneously.[2,22–24] However, except for the initial electron transfer step, such a mechanism is similar to the mechanism of the homogeneously catalysed reduction discussed earlier (Scheme 2), although the second electron transfer step involves the $CO_2^{\bullet -}$ radical anion instead of the radical anion of the catalyst. Qualitatively, it seems unlikely therefore that the reaction sequence in Scheme 1 should lead to the formation of significant amounts of CO, while the set of reactions in Scheme 2 leads exclusively to oxalate. The problem can be put in quantitative terms as follows. For the disproportionation mechanism depicted in Scheme 1, the product selection parameter is $\rho_{disp} = (K_2 k_3/k_1)[CO_2]$ and the yields of CO and oxalate are given by:[23]

$$Y^{CO} = 1 - Y^{oxalate} = \rho_{disp}/(1 + \rho_{disp})$$

Fig. 4 shows an attempt to fit the product distribution data at 0 °C (Table 2) with the theoretical predictions for the disproportionation mechanism. It is seen that the fit is not satisfactory, the experimental variation of the CO yield with the CO_2 concentration being significantly steeper than predicted by the theoretical curve. This is a first indication against the mechanism depicted in Scheme 1. Another, more direct argument can be derived from the product distribution data at 25 °C (Table 1). Previously estimated values of K_2 and k_1 at 25 °C are 0.07 mol^{-1} dm^3 and 5×10^8 mol^{-1} dm^3 s^{-1}, respectively.[25] The value of $k_{0'}$ for a potential of −2.21 V *vs.* SCE, corresponding to the $CO_2/CO_2^{\bullet -}$ couple, is 10^4 mol^{-1} dm^3 s^{-1} [25] and thus $k_{3'} \approx 10^6$ mol^{-1} dm^3 s^{-1}. Under these conditions, log ρ_{disp} = −3.8 for the largest concentration of CO_2 (0.152 mol dm^{-3}),

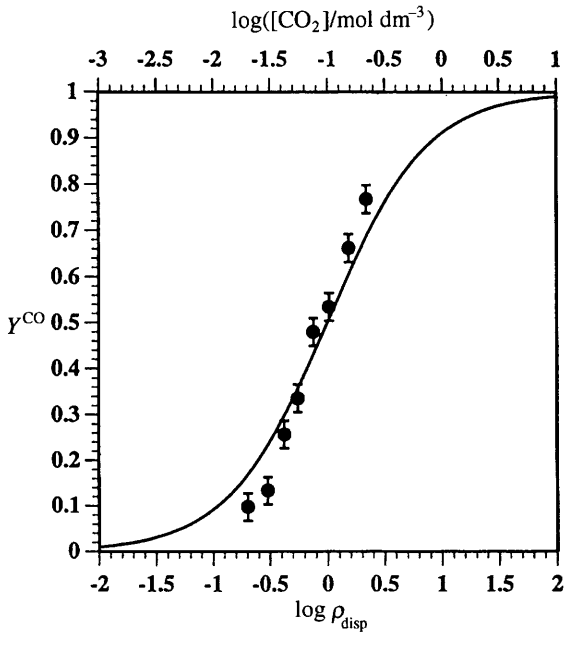

Fig. 4 Fitting of the direct electrolysis data of Table 2 (●) with the homogeneous disproportionation mechanism (solid line)

meaning that the formation of CO is predicted to be negligible while the experimental yield is 25% (Table 1).

We must therefore envisage another mechanistic possibility for the mechanism of the direct electrochemical reduction, namely the possibility of an 'ECE' mechanism,[35] *i.e.* that the reduction of the $CO_2/CO_2^{\bullet -}$ adduct would occur according to reaction (3) instead of reaction (3′) in Scheme 1. However, at the low current density employed in this work (1.6 mA cm^{-2}), the electrolysis potential is located at −2.08 V *vs.* SCE [from the current–potential curve in Fig. 2(a)], *i.e.* slightly positive to the standard potential of the $CO_2/CO_2^{\bullet -}$ couple and the standard potentials of benzonitrile and methylbenzoate. For this reason we do not expect the competition to be more in favour of CO formation in this case than it is in redox-catalysed electrolysis and than it is predicted to be for the direct electrolysis 'DISP' mechanism discussed above. It follows that the characteristics of the steps in the ECE version of Scheme 1 particularly those of step (2) should be influenced by the proximity of the electrode surface. However, in the case of a mercury electrode, specific chemical interaction with the electrode material is unlikely for the following reasons. As discussed earlier, previous observation of a two-phase Tafel plot is not an indication of significant adsorption of the reactants or intermediates but merely results from an ohmic drop effect. At mercury and lead electrodes, the reduction takes place at potentials close to the standard potential of the $CO_2/CO_2^{\bullet -}$ couple and gives rise to closely similar current–potential curves.[27] The same is true for the current–potential curves obtained upon photoinjection of electrons and capture by CO_2.[27] For the same current density and CO_2 concentration, the product distribution is the same with both electrodes. These observations point to the lack of chemical involvement of the electrode material in the reaction.

We thus propose that the formation of the CO_2–$CO_2^{\bullet -}$ adduct takes place at the electrode surface near the reaction site where the $CO_2^{\bullet -}$ radical is generated and that the ensuing steps occur as represented in Scheme 3 where the dotted line represents the potential profile from the electrode surface to the outer Helmholtz plane (OHP, where the centres of charge of the bulky tetrabutylammonium cations of the supporting electrolyte are located) and from the OHP to the solution.[37] The polarizable $CO_2^{\bullet -}$ radical anion interacts electrostatically with the negative charges on the electrode surface and, at their other end, with the tetrabutylammonium cations. This effect helps to enhance their reactivity toward the CO_2 molecules present at the electrode surface. The Lewis acidity of the latter is also likely to be enhanced by the electric field (similar to the enhancement in the acidity of Brønsted acids.[38] Thus it is likely that these two effects make the formation of the CO_2–$CO_2^{\bullet -}$ adduct [reaction (2)] more favourable than in the solution (the equilibrium constant is denoted K_2^S). We assume that the rate-determining step in the CO formation path at the electrode surface is reaction (3) with a surface rate constant k_3^S, reaction (2) acting as a pre-equilibrium. Following the representation of the reaction mechanism in Scheme 3, the current density, I, is composed of two contributions, I_1 and I_2, representing the reduction of CO_2 and of the CO_2–$CO_2^{\bullet -}$ adduct respectively ($I = I_1 + I_2$). Since, as discussed earlier, the current density is small compared with the plateau current density for the reduction of CO_2, we may assume that the CO_2 concentration is constant and equal to its bulk value throughout the system. At the electrode surface:

$$\frac{I_1}{F} = K^S K_2^S k_3^S [CO_2][CO_2^{\bullet -}]_0 - D\left(\frac{d[CO_2^{\bullet -}]}{dx}\right)_0$$

$$\frac{I_2}{F} = K^S K_2^S k_3^S [CO_2][CO_2^{\bullet -}]_0$$

where the subscript 0 stands for the plane in between the diffuse double layer and the diffusion–reaction layer. As

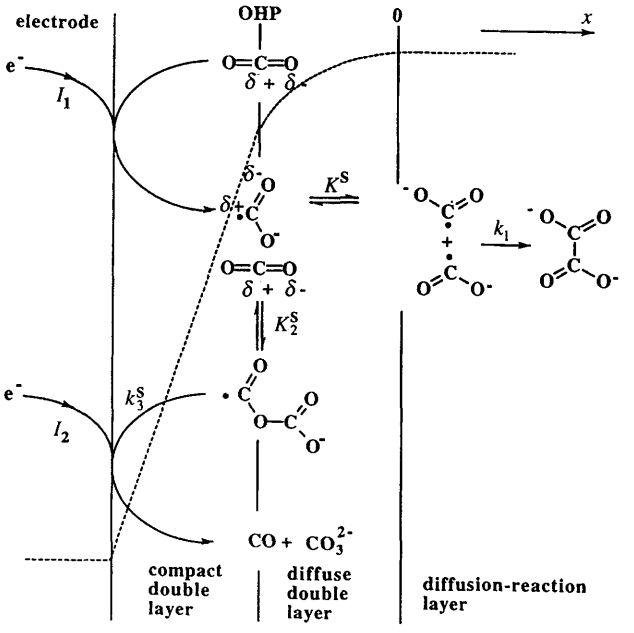

Scheme 3

results from the foregoing discussion, the oxalate formation path overruns the CO formation path in the diffusion–reaction layer:

$$\frac{d^2[CO_2^{\bullet -}]}{dx^2} = 2k_1[CO_2^{\bullet -}]^2$$

Since the dimerization [reaction (1)] is fast, the $CO_2^{\bullet -}$ profile decreases to zero within a reaction layer which is thin compared with the diffusion layer. CO is formed exclusively by surface reactions as shown in Scheme 3. The yields of CO and oxalate are obtained from the following equation.

$$Y^{CO} = 1 - Y^{oxalate} = \frac{I_2}{I_1}$$

Combination of these various equations leads to:

$$Y^{CO}\left[1 + \frac{4}{3\rho_{ECE}^{surf}}\left(\frac{Y^{CO}}{1 + Y^{CO}}\right)^{1/2}\right] = 1$$

after introduction of the product selection governing parameter,

$$\rho_{ECE}^{surf} = \frac{K^S K_2^S k_3^S [CO_2]}{(k_1 ID/F)^{1/3}}$$

As seen in Fig. 5, there is excellent agreement between the predicted and experimental variations of the CO yield with CO_2 concentration (from Table 2) which corresponds to $K^S K_2^S k_3^S / k_1 ID/F)^{1/3} = 8$ dm^6 mol^{-1} and thus $K^S K_2^S k_3^S = 0.56$ dm^7 mol^{-1} s^{-1} (K^S has no dimensions, K_2^S is in dm^6 mol^{-1}, k_3^S in dm s^{-1} as for any surface reaction).

It is also interesting to examine the variations of the yields with temperature (Table 1) in the light of the above model. In the Arrhenius plot shown in Fig. 6, the working curve in Fig. 5 has been used to derive the value of the rate parameter from the product distribution data of Table 2. It is seen that the rate parameter in Fig. 6 increases when the temperature decreases corresponding to an overall exothermic process with an enthalpy of 7.6 kcal mol^{-1}. There is little doubt that this variation is mainly due to the fact that equilibrium (2) is an exothermic reaction thanks to the electrostatic interactions that decrease in standard free energy and to the fact that it has a negative entropy.

Conclusion

There is a striking difference between direct electrolysis of CO_2 in DMF at an inert electrode, such as mercury, which

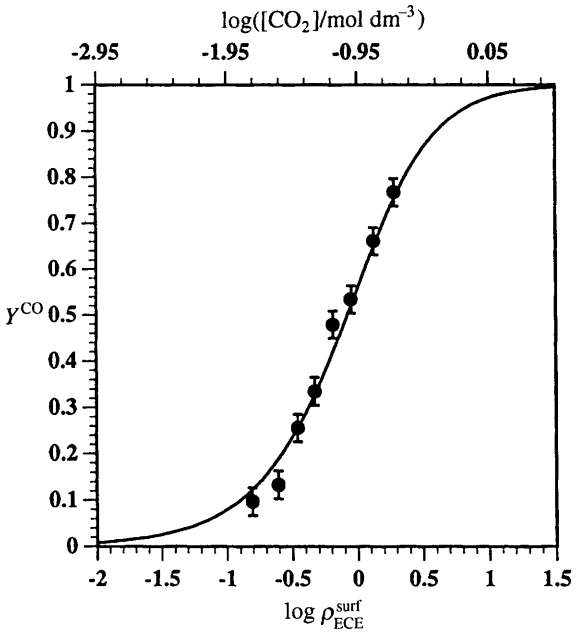

Fig. 5 Fitting of the direct electrolysis data of Table 2 (●) with the surface ECE mechanism (solid line)

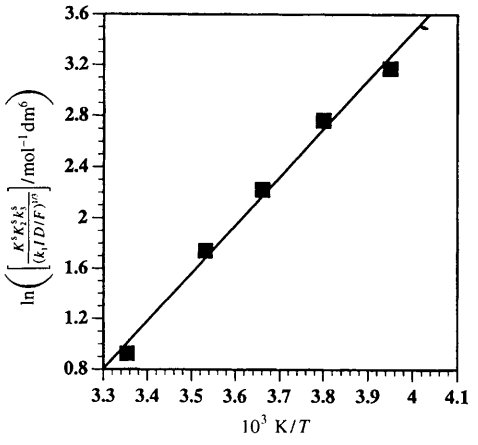

Fig. 6 Arrhenius plot derived from the data of Table 2 by means of the surface ECE model in Scheme 3

produces mixtures of CO and oxalate, and electrolysis catalysed by radical anions of aromatic esters and nitriles which produces exclusively oxalate in the same medium. Examination of previous results concerning direct electrochemical reduction and reduction by photoinjected electrons reveals that there is no significant specific interactions between reactants, intermediates, products and the electrode material when this is Hg or Pb. From these observations, and from a systematic study of the variations of the oxalate and CO yields with temperature and CO_2 concentration, a consistent mechanistic model of the direct electrochemical reduction may be proposed. It involves the formation of oxalate from the coupling of two CO_2 radical anions in solution. CO (and an equimolar amount of carbonate) is produced by reduction at the electrode of a CO_2–$CO_2^{\bullet -}$ adduct, the formation of which at the electrode surface is made exothermic by non-specific electrostatic interactions.

References

1 E. Lamy, L. Nadjo and J-M. Savéant, *J. Electroanal. Chem.*, 1977, **78**, 403.
2 J. C. Gressin, D. Michelet, L. Nadjo and J-M. Savéant, *Nouv. J. Chim.*, 1979, **3**, 545.
3 J. Fisher, T. Lehmann and E. Heitz, *J. Appl. Electrochem.*, 1981, **11**, 743.
4 S. Ikeda, T. Takagi and K. Ito, *Bull. Chem. Soc. Jpn.*, 1960. **60**, 2517.
5 M. C. Massebieau, E. Dunach, M. Troupel and J. Périchon, *New J. Chem.*, 1990, **14**, 259.
6 M. E. Royer, *C. R. Acad. Sci.*, 1870, **70**, 731.
7 A. Cohen and S. Jahn, *Ber. Dtsch. Chem. Ges.*, 1904, **37**, 2836.
8 R. Ehrenfeld, *Ber. Dtsch. Chem. Ges.*, 1905, **38**, 4138.
9 P. G. Russel, N. Kovac, S. Srinivasan and M. Steinberg, *J. Electrochem. Soc.*, 1977, **124**, 1329.
10 Y. Hori, K. Kikuchi and S. Suzuki, *Chem. Lett.*, 1985, 1695.
11 Y. Hori, A. Murata, K. Kikuchi and S. Suzuki, *J. Chem. Soc., Chem. Commun.*, 1987, 728.
12 N. V. Osetrova, Yu. B. Vasiliev, V. S. Bagotskii, R. G. Sadkova, A. F. Cherashev and A. P. Khrushch, *Elektrokhimiya*, 1984, **20**, 286.
13 D. P. Summers, S. Leach and K. W. Frese, *J. Electroanal. Chem.*, 1986, **205**, 219.
14 K. W. Frese and S. Leach, *J. Electrochem. Soc.*, 1985, **132**, 259.
15 Y. Hori, K. Kikuchi, A. Murata and S. Suzuki, *Chem. Lett.*, 1986, 897.
16 R. L. Cook, R. C. MacDuff and A. F. Sammells, *J. Electrochem. Soc.*, 1987, **134**, 2375.
17 R. L. Cook, R. C. MacDuff and A. F. Sammells, *J. Electrochem. Soc.*, 1988, **135**, 1320.
18 J. J. Kim, D. P. Summers and K. W. Frese, *J. Electroanal. Chem.*, 1988, **245**, 223.
19 M. N. Mahmood, D. Masheder and C. J. Harty, *J. Appl. Electrochem.*, 1987, **17**, 1159.
20 B. R. Eggins, E. M. Brown, E. A. McNeill and J. Grimshaw, *Tetrahedron Lett.*, 1988, **29**, 945.
21 B. R. Eggins, J. T. S. Irvine and J. Grimshaw, *J. Electroanal. Chem.*, 1989, **266**, 125.
22 C. Amatore and J-M. Savéant, *J. Am. Chem. Soc.*, 1981, **103**, 5021.
23 C. Amatore and J-M. Savéant, *J. Electroanal. Chem.*, 1994, **126**, 1.
24 C. Amatore, L. Nadjo and J-M. Savéant, *Nouv. J. Chim.*, 1984, **8**, 565.
25 A. Gennaro, A. A. Isse, J-M. Savéant, M. G. Severin and E. Vianello, *J. Am. Chem. Soc.*, in the press.
26 Y. B. Vassiliev, V. S. Bagotsky, N. V. Osetrova, O. A. Khasova and N. A. Mayorova, *J. Electroanal. Chem.*, 1985, **189**, 271.
27 Y. B. Vassiliev, V. S. Bagotsky, O. A. Khasova and N. A. Mayorova, *J. Electroanal. Chem.*, 1985, **189**, 295.
28 A. Gennaro, A. A. Isse and E. Vianello, *J. Electroanal. Chem.*, 1990, **289**, 203.
29 D. Garreau and J-M. Savéant, *J. Electroanal. Chem.*, 1984, **126**, 1.
30 I. Bhugun, D. Lexa and J-M. Savéant, *J. Am. Chem. Soc.*, 1996, **118**, 1769.
31 B. Wilhelm and R. Battino, *Chem. Rev.*, 1973, **73**, 1.
32 C. Ercolani, F. Moncelli, G. Pennasi, G. Rossi, E. Antonini and P. Acsenz, *J. Chem. Soc., Dalton Trans.*, 1981, 1120.
33 J. H. Wagenknecht, M. M. Baizer, and J. L. Chruma, *Synth. Commun.*, 1972, **2**, 215.
34 A. I. Vogel, *Textbook of Quantitative Inorganic Analysis*, Longman, London, 2nd edn., 1955, p. 275.
35 C. P. Andrieux and J-M. Savéant, *Investigation of Rates and Mechanisms of Reactions, Techniques of Chemistry*, ed. C. F. Bernasconi, Wiley, New York, 1986, vol. VI/4E, part 2, p. 305.
36 C. P. Andrieux, P. Hapiot and J-M. Savéant, *J. Electroanal. Chem.*, 1993, **49**, 299.
37 P. Delahay, *Double Layer and Electrode Kinetics*, Wiley, New York, 1965.
38 H. W. Nürnberg and G. Wolf, *J. Electroanal. Chem.*, 1969, **21**, 99.

Paper 6/02009G; *Received* 22*nd March*, 1996